



CrossMark
 click for updates

Cite this: *Nanoscale*, 2014, 6, 11106

Fluid-enabled significant enhancement and active tuning of magnetic resonances in free-standing plasmonic metamaterials

Eunice Sok Ping Leong,^{*a} Yan Jun Liu,^a Jie Deng,^a Yih Ting Fong,^b Nan Zhang,^a Si Ji Wu^a and Jing Hua Teng^{*a}

We report significantly enhanced magnetic resonance by fluid infiltration in a free-standing metamaterial that consists of metal–dielectric–metal films on an ultrathin Si₃N₄ membrane patterned with etched through nanohole arrays. When different fluids are drop-casted on the structure, the magnetic resonance has high sensitivities of 282 nm per RIU in peak shift and 12% per RIU in peak intensity change, whereas the electric resonance has nearly no changes. This work shows a promising way of using fluids to actively tune the magnetic resonance of metamaterial structures by combining with micro/nano-fluidic technologies.

Received 6th June 2014
 Accepted 17th July 2014

DOI: 10.1039/c4nr03111r

www.rsc.org/nanoscale

Introduction

Metamaterials are artificially engineered materials that possess special optical properties that natural materials do not have. They are based on resonant elements, and therefore they exhibit their desired properties only in a narrow frequency range. This spectral range is generally determined by the geometry of the structure and the properties of the constituent materials. While the geometry of the composite structure is often defined at the manufacturing stage, tunability can be achieved through the external change of the properties of the constituent materials or the geometry. Thus far, various approaches for active tuning and modulation have been explored, which include photo- and electro-excitation of free carriers,^{1–4} mechanical movement of elements,^{5,6} phase-change using chalcogenides,⁷ vanadium dioxides^{8,9} and liquid crystals,^{10–12} as well as temperature control of superconducting materials.^{13,14} A straightforward way to achieve large tunability is to infiltrate the metamaterial structures with fluids of different refractive indices. The tunability of metamaterial devices with fluids is guaranteed by three intrinsic characteristics of fluid: mobility, reconfigurability and a large range of index modulation, which can be enabled by micro/nano-fluidic technologies. We expect that combining with micro/nano-fluidic technologies, the fluid-enabling active metamaterial devices could play an important role in future nanophotonics.

The split ring resonator (SRR) is the first demonstration to exhibit negative permeability in the microwave regime.^{15,16} The

split gap in the SRR causes the induced circulating current, which is a result of the varying magnetic field, to build up charges across the gap. When the frequency of the magnetic field increases, the gap causes the applied magnetic field and induced current to be out-of-phase and results in a negative response.¹⁷ To push the negative response to the visible-near infrared range, the SRR structure has been simplified to the U-shape SRR or the cut-wire pair to reduce the periodicity and dimensions of each structure.^{18–23} The perforated metal–dielectric–metal (MDM) structure is a further simplified fishnet design that exhibits both negative permittivity and permeability in the optical range.²⁴ So far, the smallest structure that is demonstrated has a period of 220 nm with a square hole of length 80 nm.²⁵ The structure is fabricated using the standard lift-off technique, which faces great challenges when the feature size of the MDM structure goes down to the deep subwavelength scale. Recently, we demonstrated a much simpler process to fabricate the MDM perforated structures on a free-standing Si₃N₄ membrane. The method involves fabricating a nano-stencil using the etching method and directly evaporating the multilayer films on the stencil to form the MDM perforated structure.²⁶ Such a fabrication method has been widely adopted for metallic nanohole arrays based on-chip sensing as it has the additional advantage of flow through sensing from the perforated holes.²⁷

In this paper, we will study the effect of the dielectric surroundings on the optical properties of the free-standing MDM metamaterial structures. The metamaterial structure is formed by layered deposition of Au/MgF₂/Au on a free-standing, holey-patterned ultrathin Si₃N₄ membrane. By drop-casting different fluids of known refractive indices on the metamaterial structures, significant enhancement of magnetic resonances is observed. In addition, the magnetic resonance red-shifts with

^aInstitute of Materials Research and Engineering, Agency for Science, Technology and Research (A*STAR), 3 Research Link, Singapore 117602, Singapore. E-mail: leonge@imre.a-star.edu.sg; jh-teng@imre.a-star.edu.sg

^bNational Junior College, 37 Hillcrest Road, Singapore 288913, Singapore

the increase of the refractive index of the surrounding fluids. This method shows a promising way to develop fluid-enabled active metamaterial devices.

Methods

Sample fabrication

The details on fabricating the nanostencil, which is a free-standing nanohole on the Si_3N_4 membrane, can be found in ref. 26 and the fabrication steps are illustrated in Fig. 1(a). Briefly, a 100 nm thick free-standing Si_3N_4 membrane was first fabricated followed by e-beam lithography (ELS-7000, ELIONIX) and reactive ion-etching (Plasmalab 80plus, Oxford) processes to create holes of diameter 120 nm with a square period of 200 nm on the membrane. The working size of the pattern was $20 \times 20 \mu\text{m}^2$. The final step was to evaporate alternating Au and MgF_2 layers to form a MDM film using an e-beam evaporator (Denton Vacuum, Explorer). The thickness of Au and MgF_2 layers was 40 nm and 45 nm, respectively. To minimize the roughness introduced by metal and dielectric deposition, the evaporation rate of both Au and MgF_2 was set to be 0.5 nm s^{-1} .

Spectral measurement

Unpolarized transmittance spectra at normal incidence were recorded using a UV-Vis-NIR microspectrophotometer (QDI 2010™, Craic) with a 75 W broadband xenon light source. The probe light beam was focused on the silicon nitride layer of the sample through a condenser and the transmitted light was collected from the Au surface through an objective lens (magnification: 36×; numerical aperture: 0.5). The detection area was $7.1 \times 7.1 \mu\text{m}^2$ and the transmission spectra were normalized with respect to unblocked, free-space (*i.e.*, air) transmission.

To vary the dielectric environment of the sample, different fluids of known refractive indices were drop-casted on the Au side of the patterned region. A cover-slip glass was placed on the fluid so that it would slow down the evaporation of fluid and also prevent the fluid to form a droplet on the pattern and affect the transmittance data. An illustration of the measurement is shown in Fig. 1(b). After measurement, the sample was rinsed with deionized (DI) water and blown dry with a nitrogen gun. The transmittance measurements were repeated until the spectrum was stable and returned to nearly the original peak position. The fluids used for drop-casting were methanol ($n = 1.328$), DI water ($n = 1.333$), ethanol ($n = 1.361$) and isopropanol ($n = 1.377$).

Optical simulation

To model the optical properties of the free-standing MDM metamaterial structures, we carried out the finite-difference time-domain (FDTD) simulation using a commercial software (Lumerical). The thicknesses of the Si_3N_4 , Au and MgF_2 layers were 100 nm, 40 nm, and 45 nm respectively. Conical holes with a diameter of 120 nm at the bottom Si_3N_4 layer and with a diameter of 80 nm at the top Au layer with period 200 nm in the x - y range were defined in the simulation. Periodic boundary conditions were applied in the x - y plane and the perfectly matched layer (PML) boundary condition was applied in the z -direction. Plane wave was impinging from the bottom, reaching the Si_3N_4 layer first. A mesh of 1 nm was used to simulate the conical hole. The dispersion of gold was based on the Johnson and Christy model in ref. 28 found in the material library of the software. To simulate the optical properties of the structure under different refractive indices, the background index of the simulation and the refractive index of the conical hole were set to the index of the fluid of interest.

Results and discussion

The SEM image of the nanohole pattern on the Si_3N_4 membrane is shown in Fig. 2(a). The Si_3N_4 surface is smooth and the nanoholes have a diameter of 120 nm. On the other side of the membrane that is coated with the MDM layers, the size of the nanoholes shrunk to 80 nm as shown in Fig. 2(b). It is a well-known fact that when evaporating on a nanostencil, the deposited material will tend to clog the hole, resulting in a smaller hole size.^{29,30} Likewise, this phenomenon is also observed in the fabricated sample. Tiny grains were also

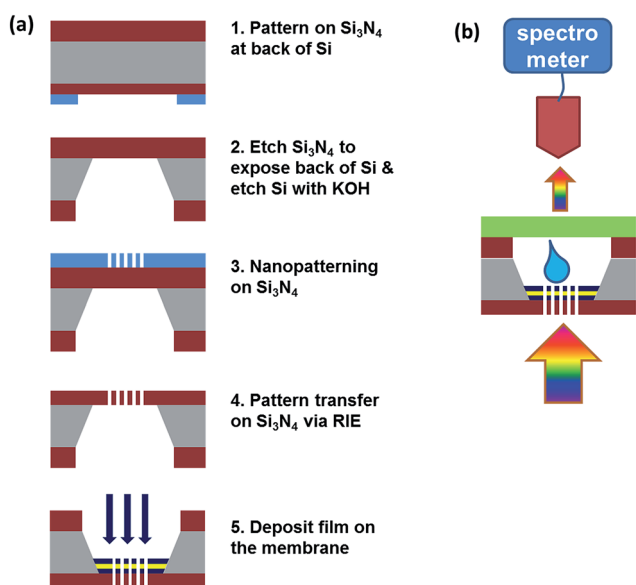


Fig. 1 (a) Fabrication steps of preparing free-standing MDM perforated structures on the Si_3N_4 membrane. (b) Illustration of optical measurement with the drop-casted fluid.

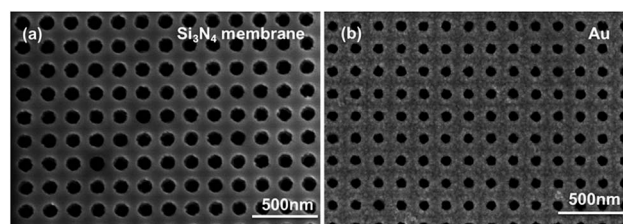


Fig. 2 SEM images of the fabricated sample on (a) the Si_3N_4 surface and on (b) the Au surface.

observed on the surface as metals tend to grow in Volmer-Weber mode and is common in MDM stacks.^{31,32}

The shrinking of holes and the presence of some materials at the inner edge of the holes suggest that a conical MDM hole is formed. Fig. 3(a) shows a schematic of how the structure may look like and Fig. 3(b) shows the measured transmittance spectrum of the sample. Two Lorentzian spectra are observed from the Lorentzian fitting of the spectrum (a dotted green line and a dotted blue line; the dotted red line is the summation of the dotted green and blue curves). To have an in-depth understanding on the origins of these two peaks, we performed FDTD simulation of the structure. Fig. 3(c) shows the index profile of one unit cell in our simulation. The simulated transmittance spectrum as shown in Fig. 3(d) is similar to the experimental result, except that the simulated spectrum is narrower than the experimental one. The broadening of the spectrum is mainly due to the larger scattering loss caused by the rougher MDM surface in the experiment as opposed to the ideally smooth surface set in the simulation.

Our free-standing MDM perforated structures can be considered as fishnet metamaterials, which look similar to the reported structures based on e-beam lithography.²⁵ Such a fishnet structure usually has two optical resonances. One is the electric resonance that is formed by the metallic strips aligned in the direction of the electric field. The other one is the magnetic resonance that comes from the coupling of the upper and lower layers in the magnetic strips.²⁴ In our case, these two resonances correspond to the two peaks, T1 and T2 denoted in the spectra. This can be further confirmed by the mapped magnetic field distribution and electric displacement plot at these two resonance wavelengths, as shown in Fig. 4(a) and (b). The electric displacement, as represented by the arrows in the figures, is predominantly aligned along the MDM layers at T1

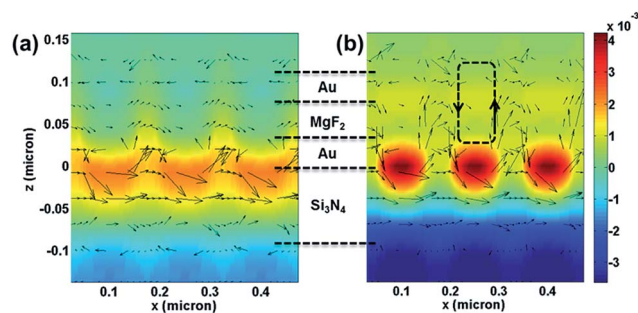


Fig. 4 The magnetic field (H_y) distribution and the electric displacement field vector (*i.e.*, the electric current) plot indicated by the colormap and arrows, respectively, for (a) T1 ($\lambda = 510$ nm) and (b) T2 ($\lambda = 550$ nm) in the simulated transmittance spectrum in Fig. 3(d).

($\lambda = 510$ nm). At T2 ($\lambda = 550$ nm), the electric displacement forms a resonant loop in the highlighted region and induces an artificial magnetic moment. As a result, a strong magnetic field is observed in the MDM stack. Therefore the response at T1 is attributed to the electric resonance whereas the response at T2 is due to the magnetic resonance of the structure. The retrieved refractive index at T2 is calculated to be ~ 0.6 . We also note an intense magnetic field at the interface between the Si_3N_4 and the Au layer. This is due to the SPPs propagating along the metal-dielectric interface. As light is trapped at the interface, it will not contribute to the transmission.

Fig. 5(a) shows the optical spectra when different fluids were drop-casted on the Au surface of the structure. The spectrum of the structure in air was also plotted for comparison. Compared to the as-deposited MDM structure in air, a distinct difference in the spectrum is the emergence of the strong magnetic resonance when immersing the structure in the higher refractive index fluids. From Fig. 5(a), it is clear that the magnetic

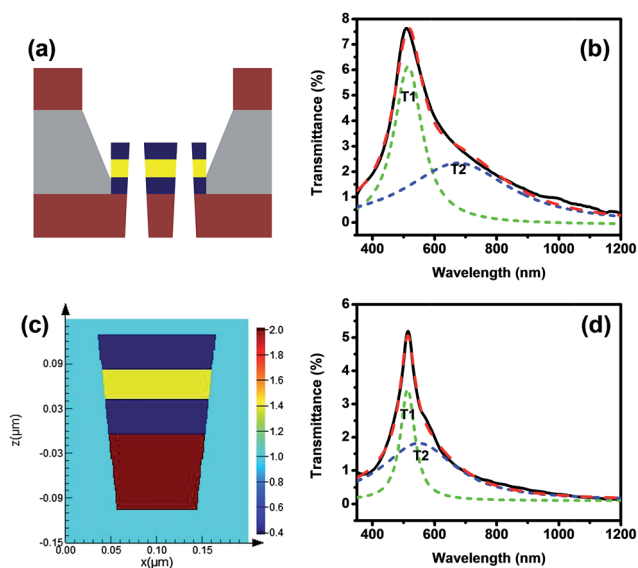


Fig. 3 (a) Schematic of how the structure looks like based on the SEM images. (b) Measured transmittance spectrum of the structure. (c) Index profile of one unit cell of the simulated structure. (d) Simulated transmittance spectrum.

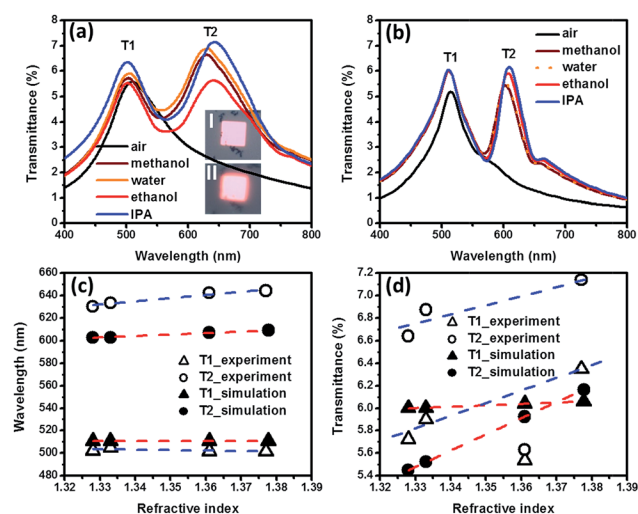


Fig. 5 Experimental (a) and simulated (b) transmittance of the sample when different fluids are used. The insets in (a) show the CCD images of the patterned region in air (I) and water (II). Plot of the wavelength position (c) and intensity (d) of the peaks with respect to the refractive index of the fluids derived from (a) and (b).

resonance peak shifts with the changes of the refractive index while the electric resonance peak position is almost unaltered. For the magnetic resonance, in addition to the peak shift, we also observed a dramatic increase in the peak transmittance. The significant transmittance increase is also confirmed under a CCD camera. The inset of Fig. 5(a) shows the CCD images of the patterned region before (inset I) and after (inset II) water drop-casting under the same observing conditions. We can see that the CCD image shows a much brighter color after the water was drop-casted on the patterned region (picture II). We also note that the captured CCD image after water drop-casting is saturated due to the strong transmission enhancement, which does not indicate the expected reddish color. However, the image appears more reddish along the pattern edges due to the higher contrast, which gives the clue of the expected reddish color. These changes in the peak position and transmittance show that the magnetic resonance of the metamaterial structure depends on not only the geometry of the structure and its composite materials but also on the refractive index of the surrounding medium. This agrees well with the fact that the surrounding refractive index affects the coupling strength of the top and bottom metallic layers. When fluids are drop-casted on the structures, it reduces the refractive index contrast and thereby reduces the plasmonic losses. Hence, this boosts the optical transmission. As for the electric resonance, it mainly depends on the electric permittivity of gold. Furthermore, the electric resonance for this structure is near the inter-band transition of gold and therefore, its response to the surrounding refractive index is small. Similar trends have been further confirmed from the simulated transmittance spectra with the same surrounding fluids used in our experiment, as shown in Fig. 5(b). It is worth mentioning that once the drop-casted fluids evaporate, the transmittance spectra will return to the original state, indicating that one can actively switch/tune the magnetic resonance by using the fluids. Especially, by combing with the micro/nano-fluidic technologies, active metamaterial devices can be further developed.

To have a closer look at how the peaks change with respect to different fluids, we plot the position and transmission intensity of both electric and magnetic resonance peaks as a function of the refractive index of the different fluids. Fig. 5(c) and (d) show the peak changes in terms of position and intensity, respectively, where the data are retrieved from Fig. 5(a) and (b). On the peak shift in Fig. 5(c), it is observed that experimentally, the wavelength position of T1 is at 503 ± 1.5 nm and does not shift much with the increase of the refractive index. As for T2, the peak position changes from 630.4 nm to 644.2 nm when the fluid is changed from methanol to isopropanol. It is noted that this change is linear with respect to the index, which corresponds to a bulk refractive index sensitivity of $\Delta\lambda/\Delta n = 282$ nm per RIU. Such a sensitivity is comparable to the plasmonic sensors,^{33,34} indicating that this free-standing MDM metamaterial structure is also potentially useful for biosensing applications. The result is similar to the one simulated whereby T1 does not change in position and T2 red-shifts linearly with the higher refractive index. We believe that the sensitivity can be further improved by reducing the loss and enhancing the magnetic resonance of the

structure *via* structural^{24,35} and materials engineering.^{21–23} Upon change of the peak transmittance in Fig. 5(d), experimental and simulated results show that the transmittance of both electric and magnetic resonant peaks is increased. However, the magnetic resonance peak is much more sensitive to the surrounding index change as compared to the electric one. We also observe that the data on ethanol deviate from the line trend. This is because ethanol has the lowest surface tension among the solvents used. Hence it has the highest wetting ability and has a higher tendency to seep through the holes. As a result, it is highly possible that ethanol does not fully cover the patterned area and results in a less-than-expected transmission enhancement in the spectrum. From our experiments, the magnetic resonance has a sensitivity of $\Delta T/\Delta n = 12\%$ per RIU, which is ~ 5 times higher than that of the electric resonance (2.3% per RIU). Such a transmission-based sensitivity gives the fact that a variation in the refractive index of the surrounding medium provides obvious modification of transmittance at a certain wavelength, indicating that it is also possible to develop single wavelength sensing application using the magnetic optical resonance. Compared with sensing configurations based on the measurement of the spectral shift of a resonance, such a single wavelength detecting scheme will be much simpler and less time-consuming.

It is worth mentioning that our free-standing metamaterial with etched through nanoholes has a major advantage for the transmission-based detecting/sensing applications compared to those with dead-end nanoholes due to the significant enhancement of magnetic resonances. The etched through nanoholes allow fluids to seep through the perforated holes and wet the outer surface, hence enabling significant enhancement and high sensitivities for the magnetic resonances. To further confirm that the significant enhancement of the magnetic resonance is caused by the etched through nanoholes, we therefore numerically compared our free-standing metamaterial structures with three cases of fluid infiltration: (I) fluid is only on top of the metal surface; (II) fluid seeps inside nanoholes; and (III) fluid seeps through the nanoholes. The insets in Fig. 6 illustrate the index profiles of the assumed three cases, in which DI water is taken as an example. Fig. 6 shows the simulated transmission spectra of the corresponding three cases. We can see that the magnetic resonance peak evolves drastically when the DI water seeps from the top to the bottom of the free-standing metamaterial. With the DI water just on the top surface (case I), only a slight shoulder appears from the original spectrum in the air. When the DI water seeps inside the nanoholes (case II), a pronounced magnetic resonance peak evolves from the shoulder with a clear red-shift. After the DI water seeps through the nanoholes (case III), the peak intensity is further enhanced although there is no clear red-shift. For those similar metamaterials on a solid substrate with dead-end nanoholes, the DI water can at most seep inside the nanoholes like in case II. In contrast, the free-standing metamaterial with the etched through nanoholes will allow the fluids to seep through easily and hence further enhance the magnetic resonance. This could be a distinct advantage of the free-standing metamaterials with etched through nanoholes for the transmission-based detecting/sensing applications.

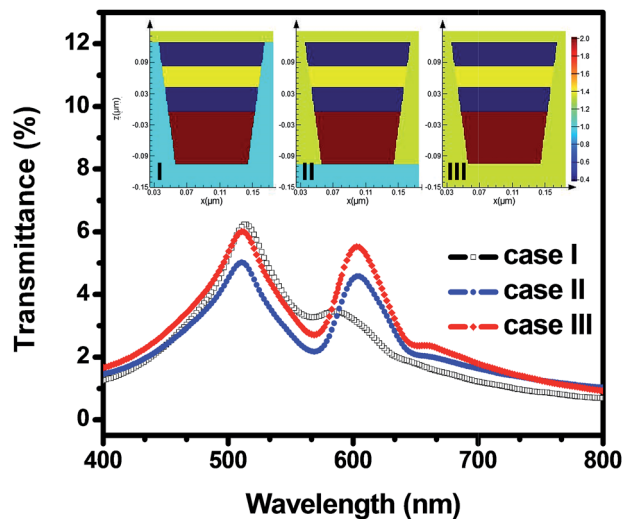


Fig. 6 Simulated transmission spectra of three different cases of fluid infiltration: (I) fluid is only on top of the metal surface; (II) fluid seeps inside nanoholes; and (III) fluid seeps through the nanoholes.

Conclusions

To summarize, we have achieved significant enhancement of magnetic resonances in a free-standing metamaterial with fluid infiltration. Moreover, the magnetic resonance peak red-shifts linearly with the increase of the refractive index of the surrounding fluid. Both experimental and simulation results have confirmed that the magnetic resonance is strongly sensitive surroundings' index. We have demonstrated high sensitivities of 282 nm per RIU in peak shift and 12% per RIU in peak intensity change for the magnetic resonance in our free-standing metamaterial sample. A major advantage of this free-standing fishnet metamaterial is that it has etched through nanoholes which allow fluids to seep through and hence enable significant enhancement and high sensitivities for the magnetic resonances. In addition, the fabrication of such an MDM perforated structure on a free-standing Si_3N_4 membrane is much simpler compared to the conventional fabrication techniques that involve the lift-off process. This method only requires patterning on the thin Si_3N_4 layer which can be easily etched using the standard reactive ion etching technique. This work shows a promising way of using fluids to actively tune the magnetic resonance of metamaterial structures, in terms of both the wavelength position and peak intensity, which can be realized using micro/nano-fluidic technologies.

Acknowledgements

This work was financially supported by the Agency for Science, Technology and Research (A*STAR), under the grant no. 0921540099 and 0921540098.

Notes and references

1 H.-T. Chen, J. F. O'Hara, A. K. Azad, A. J. Taylor, R. D. Averitt, D. B. Shrekenhamer and W. J. Padilla, *Nat. Photonics*, 2008, **2**, 295.

- 2 H.-T. Chen, W. J. Padilla, M. Cich, A. Azad, R. D. Averitt and A. Taylor, *Nat. Photonics*, 2009, **3**, 148.
- 3 L. Y. Deng, J. H. Teng, H. W. Liu, Q. Y. Wu, J. Tang, X. H. Zhang, S. A. Maier, K. P. Lim, C. Y. Ngo, S. F. Yoon and S. J. Chua, *Adv. Opt. Mater.*, 2012, **1**, 128.
- 4 D. Shrekenhamer, S. Rout, A. C. Strikwerda, C. Bingham, R. D. Averitt, S. Sonkusale and W. J. Padilla, *Opt. Express*, 2011, **19**, 9968.
- 5 J. Y. Ou, E. Plum, L. Jiang and N. I. Zheludev, *Nano Lett.*, 2011, **11**, 2142.
- 6 W. M. Zhu, A. Q. Liu, T. Bourouina, D. P. Tsai, J. H. Teng, X. H. Zhang, G. Q. Lo, D. L. Kwong and N. I. Zheludev, *Nat. Commun.*, 2012, **3**, 1274.
- 7 B. Gholipour, J. Zhang, K. F. MacDonald, D. W. Hewak and N. I. Zheludev, *Adv. Mater.*, 2013, **25**, 3050.
- 8 X.-Y. Peng, B. Wang, J. H. Teng, J. B. Kana Kana and X. H. Zhang, *J. Appl. Phys.*, 2013, **114**, 163103.
- 9 M. Seo, J. Kyoung, H. Park, S. Koo, H.-S. Kim, H. Bernien, B. J. Kim, J. H. Choe, Y. H. Ahn, H.-T. Kim, N. Park, Q.-H. Park, K. Ahn and D.-S. Kim, *Nano Lett.*, 2010, **10**, 2064.
- 10 S. M. Xiao, U. K. Chettiar, A. V. Kildishev, V. Drachev, I. C. Khoo and V. M. Shalaev, *Appl. Phys. Lett.*, 2009, **95**, 033115.
- 11 A. Minovich, D. N. Neshev, D. A. Powell, I. V. Shadrivov and Y. S. Kivshar, *Appl. Phys. Lett.*, 2010, **96**, 193103.
- 12 Y. J. Liu, G. Y. Si, E. S. P. Leong, N. Xiang, A. J. Danner and J. H. Teng, *Adv. Mater.*, 2012, **24**, OP131.
- 13 M. Ricci, N. Orloff and S. M. Anlage, *Appl. Phys. Lett.*, 2005, **87**, 034102.
- 14 H.-T. Chen, H. Yang, R. Singh, J. F. O'Hara, A. K. Azad, S. A. Trugman, Q. X. Jia and A. J. Taylor, *Phys. Rev. Lett.*, 2010, **105**, 247402.
- 15 J. B. Pendry, A. J. Holden, D. J. Robbins and W. J. Stewart, *IEEE Trans. Microwave Theory Tech.*, 1999, **47**, 2075.
- 16 D. R. Smith, W. J. Padilla, D. C. Vier, S. C. Nemat-Nasser and S. Schultz, *Phys. Rev. Lett.*, 2000, **84**, 4184.
- 17 W. J. Padilla, D. N. Basov and D. R. Smith, *Mater. Today*, 2006, **9**, 28.
- 18 G. Dolling, C. Enkrich, M. Wegener, J. F. Zhou, C. M. Soukoulis and S. Linden, *Opt. Lett.*, 2005, **30**, 3198.
- 19 W. S. Cai, U. K. Chettiar, H.-K. Yuan, V. C. de Silva, A. V. Kildishev, V. P. Drachev and V. M. Shalaev, *Opt. Express*, 2007, **15**, 3333.
- 20 E. S. P. Leong, Y. J. Liu, C. C. Chum and J. H. Teng, *Plasmonics*, 2013, **8**, 1221.
- 21 X. L. Xu, B. Peng, D. H. Li, J. Zhang, L. M. Wong, Q. Zhang, S. J. Wang and Q. H. Xiong, *Nano Lett.*, 2011, **11**, 3232.
- 22 L. Y. M. Tobing, L. Tjahjana, D. H. Zhang, Q. Zhang and Q. H. Xiong, *Adv. Opt. Mater.*, 2014, **2**, 280.
- 23 L. Y. M. Tobing, L. Tjahjana, D. H. Zhang, Q. Zhang and Q. H. Xiong, *Sci. Rep.*, 2013, **3**, 2437.
- 24 S. Zhang, W. J. Fan, K. J. Malloy and S. R. J. Brueck, *Opt. Express*, 2005, **13**, 4922.
- 25 S. M. Xiao, U. K. Chettiar, A. V. Kildishev, V. P. Drachev and V. M. Shalaev, *Opt. Lett.*, 2009, **34**, 3478.
- 26 E. S. P. Leong, J. Deng, Y. J. Liu and J. H. Teng, *Appl. Phys. A: Mater. Sci. Process.*, 2014, DOI: 10.1007/s00339-014-8461-9.
- 27 C. Escobedo, *Lab Chip*, 2013, **13**, 2445.

- 28 P. B. Johnson and R. W. Christy, *Phys. Rev. B: Solid State*, 1972, **6**, 4370.
- 29 M. Kölbl, R. Willem Tjerkstra, J. Brugger, C. J. M. Van Rijn, W. Nijdam, J. Huskens and D. N. Reinhoudt, *Nano Lett.*, 2002, **12**, 1339.
- 30 M. M. Deshmukh, D. C. Ralph, M. Thomas and J. Silcox, *Appl. Phys. Lett.*, 1999, **75**, 1631.
- 31 E. S. P. Leong, Y. J. Liu, B. Wang and J. H. Teng, *ACS Appl. Mater. Interfaces*, 2011, **3**, 1148.
- 32 W. Chen, M. D. Thoreson, A. V. Kildishev and V. M. Shalaev, *Laser Phys. Lett.*, 2010, **7**, 677.
- 33 A. De Leebeeck, L. K. Swaroop Kumar, V. de Lange, D. Sinton, R. Gordon and A. G. Brolo, *Anal. Chem.*, 2007, **79**, 4094.
- 34 Z. Y. Cai, Y. J. Liu, X. M. Lu and J. H. Teng, *J. Phys. Chem. C*, 2013, **117**, 9440.
- 35 Z. Ku and S. R. J. Brueck, *Opt. Express*, 2007, **15**, 4515.